Inorg. Chem. **2005**, *44*, 8216–8222

Oxomolybdenum Tetrathiolates with Sterically Encumbering Ligands: Modeling the Effect of a Protein Matrix on Electronic Structure and Reduction Potentials

Rebecca L. McNaughton,[§] Sujit Mondal,[‡] Victor N. Nemykin,[‡] Partha Basu,*[,‡] and Martin L. Kirk*[,†]

Department of Chemistry, The University of New Mexico, MSC03 2060, 1 University of New Mexico, Albuquerque, New Mexico 87131-0001, and Department of Chemistry and Biochemistry, Duquesne University, Pittsburgh, Pennsylvania 15282

Received December 16, 2004

The effect of sterically encumbering ligands on the electronic structure of oxomolybdenum tetrathiolate complexes was determined using a combination of electronic absorption and magnetic circular dichroism spectroscopies, complimented by DFT bonding calculations, to understand geometric and electronic structure contributions to reduction potentials. These complexes are rudimentary models for a redox-active metalloenzyme active site in a protein matrix and allow for detailed spectroscopic probing of specific oxomolybdenum–thiolate interactions that are directly relevant to Mo–$S_{cysteine}$ bonding in pyranopterin molybdenum enzymes. Data are presented for three *para*-substituted oxomolybdenum tetrathiolate complexes ([PPh_4][MoO(*p*-SPhCONHCH_3)$_4$], [PPh_4][MoO(*p*-SPhCONHC($CH_2O(CH_2)_2$-CN)$_3$)$_4$], and [PPh_4][MoO(*p*-SPhCONHC($CH_2O(CH_2)_2COOCH_2CH_3$)$_3$)$_4$]). The Mo(V/IV) reduction potentials of the complexes in DMF are −1213, −1251, and −1247 mV, respectively. The remarkably similar electronic absorption and magnetic circular dichroism spectra of these complexes establish that the observed reduction potential differences are not a result of significant changes in the electronic structure of the [MoOS_4]$^-$ cores as a function of the larger ligand size. We provide evidence that these reduction potential differences result from the driving force for a substantial reorganization of the O–Mo–S–C dihedral angle upon reduction, which decreases electron donation from the thiolate sulfurs to the reduced molybdenum center. The energy barrier to favorable O–Mo–S–C geometries results in a reorganizational energy increase, relative to [MoO$(SPh)_4]^{-/2-}$, that correlates with ligand size. The inherent flexible nature of oxomolybdenum–thiolate bonds indicate that thiolate ligand geometry, which controls Mo–S covalency, could affect the redox processes of monooxomolybdenum centers in pyranopterin molybdenum enzymes.

Introduction

Understanding the effects of a protein matrix on metal ion active site electronic structure and redox potentials is a fundamental goal in bioinorganic chemistry. As such, the encapsulation of iron−sulfur clusters and porphyrins by dendritic organic moieties has recently been employed as a strategy to model biological metalloprotein redox centers.[1,2] Appreciable changes in many of the physical properties of redox-active cores, including the reduction potential, polarity, solubility, pK_a of functional groups, and photochemical behavior, are observed upon increasing the steric bulk of the ligand set and encapsulating the metal center.[1−4] Similarly, complexes with sterically encumbering ligands, modeling specific metal−ligand interactions present in the active sites of pyranopterin molybdenum enzymes, have recently been synthesized to test specific hypotheses regarding electron-transfer regeneration of the enzyme active sites.[5] Numerous crystal structures of pyranopterin molybdenum enzymes have established that their active sites are deeply buried in the surrounding protein and that endogenous redox

* Author to whom correspondence should be addressed. E-mail: mkirk@unm.edu.
† The University of New Mexico.
‡ Duquesne University.
§ Present address: Department of Chemistry, Northwestern University, Evanston, IL 60208.

(1) Smith, D. K.; Diederich, F. *Chem.*—Eur. J. **1998**, *4*, 1353.
(2) Gorman, C. B.; Smith, J. C. *Acc. Chem. Res.* **2001**, *34*, 60.
(3) Vogtle, F.; Gestermann, S.; Hesse, R.; Schwierz, H.; Windisch, B. *Prog. Polym. Sci.* **2000**, *25*, 987.
(4) Smith, D. K.; Diederich, F. *Top. Curr. Chem.* **2000**, *210*, 183.
(5) Mondal, S.; Basu, P. *Inorg. Chem.* **2001**, *40*, 192.

10.1021/ic0482281 CCC: $30.25
Published on Web 10/12/2005

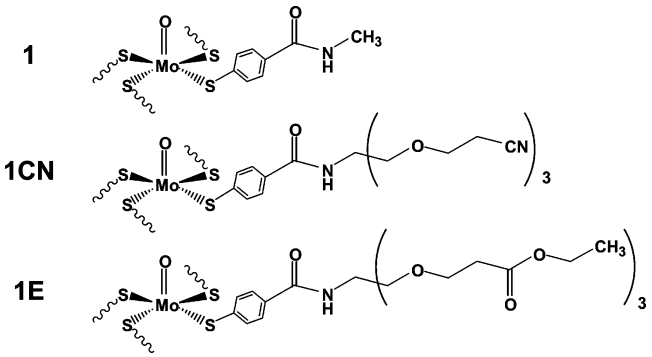

Figure 1. Structures and abbreviations for the molybdenum tetrathiolate complexes used in this study. For clarity, only one complete benzenethiolate ligand is shown for each complex.

Chart 1. Consensus Structures of the Three Families of Pyranopterin Molybdenum Enzymes in Their Electron-Transfer Relevant Geometries

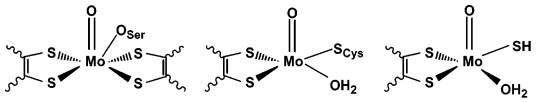

cofactors and key amino acid residues are often hydrogen-bonded to ligands of the active site.[6,7] Thus, electron-transfer processes between the molybdenum active site and both endogenous and exogenous redox-active cofactors are believed to be greatly influenced by the surrounding protein matrix. The complexes in this study possess a $[Mo^{V}OS_4]^-$ core consisting of a single terminal oxo ligand and four *para*-substituted benzenethiolate sulfur donors, as shown in Figure 1.[5] Although these complexes are not exact structural models for one particular molybdenum enzyme active site, they possess sterically encumbered $[Mo^{V}O(\text{benzenethiolate})_4]^-$ cores of relatively high symmetry, for which the electronic structure is well-understood,[8−10] and this allows for detailed spectroscopic probing with respect to oxomolybdenum−thiolate interactions in pyranopterin molybdenum enzymes. The monooxo $Mo^{V/IV}$ reduction potentials of these complexes are of specific relevance to the redox processes that occur at the monooxo molybdenum active sites of the xanthine oxidase, sulfite oxidase, and dimethyl sulfoxide reductase enzyme families during the electron-transfer half-reaction of their catalytic cycles (Chart 1).[6,11]

The most significant change in the physical properties of the sterically encumbered complexes **1CN** and **1E** relative to **1** is the ∼36 mV difference in their reduction potentials (in DMF), which are nearly double the ∼20 mV shift observed for dendrimer-encapsulated iron−sulfur clusters.[12,13] As the length of the *para* substituent on the phenyl ring is increased, the reduction potentials decrease ($E_{1/2}$ = −1213 mV for **1**, −1251 mV for **1CN**, and −1247 mV for **1E**) and the difference between the reduction and oxidation wave maxima increases (ΔE_p = 68 mV for **1**, 167 mV for **1CN**, and 335 mV for **1E**).[14] Here we probe the effect of steric bulk on the electronic structure of $[MoOS_4]^-$ cores and describe the origin of the observed modulation of their reduction potentials.

Experimental Procedures

General Procedures. Synthesis and characterization of $[PPh_4][MoO(p\text{-}SPhCONHCH_3)_4]$ (**1**), $[PPh_4][MoO(p\text{-}SPhCONHC(CH_2O(CH_2)_2CN)_3)_4]$ (**1CN**), and $[PPh_4][MoO(p\text{-}SPhCONHC(CH_2O(CH_2)_2COOCH_2CH_3)_3)_4]$ (**1E**) is described elsewhere.[14] $[PPh_4][MoO(SPh)_4]$ was prepared as previously reported.[15] All spectroscopic samples were prepared in a glovebox/bag under N_2 using degassed and dried solvents.

Electronic Absorption Spectroscopy. Electronic absorption spectra were collected on a Hitachi U-3501 UV−vis−NIR spectrophotometer using a double-beam configuration at 2.0 nm resolution. Low-temperature (10 K) spectra were collected using a Janis STVP-100 continuous-flow cryostat mounted in a custom designed cradle assembly, and the sample temperature was monitored with a Lakeshore silicon-diode (PT-470). Polymer thin film samples were prepared by dissolving the compounds in acetonitrile, mixing this solution with a saturated solution of polystyrene in toluene, and pouring this mixture onto a flat glass plate to evaporate the solvent under a stream of N_2 in a glovebag.

Magnetic Circular Dichroism (MCD) Spectroscopy. Low-temperature MCD spectra were collected on a system consisting of a Jasco J600 CD spectropolarimeter employing Hamamatsu photomultiplier tubes of either S-1 or S-20 response, an Oxford Instruments SM4000-7T superconducting magneto−optical cryostat (0−7 T, 1.4−300 K), and an ITC503 Oxford Instruments temperature controller. The spectrometer was calibrated for circular dichroism intensity with camphorsulfonic acid, and the wavelength was calibrated using Nd-doped glass. Polymer thin film samples were prepared as described above and secured in a custom designed sample cell. Depolarization of the incident radiation was examined by comparing the intrinsic circular dichroism of a standard Ni (+)-tartarate solution positioned in front of and then in back of each sample. The spectra were collected at 2.0 nm resolution at a temperature of 5 K in an applied magnetic field of 7 T.

Electronic Structure Calculations. Density functional (DFT) calculations were performed using the Gaussian 98W software package.[16] Unless noted otherwise, all calculations employed Becke's three-parameter hybrid exchange functional and the 6-31G

(6) Hille, R. *Chem. Rev.* **1996**, *96*, 2757.
(7) Dobbek, H.; Huber, R. *Met. Ions Biol. Syst.* **2002**, *39*, 227.
(8) McNaughton, R. L.; Tipton, A. A.; Rubie, N. D.; Conry, R. R.; Kirk, M. L. *Inorg. Chem.* **2000**, *39*, 5697.
(9) McNaughton, R. L. Electronic Structure Studies of Oxomolybdenum−Thiolate Complexes Related to Pyranopterin Molybdenum Enzymes. Ph.D. Dissertation, The University of New Mexico, Albuquerque, NM, 2002.
(10) McMaster, J.; Carducci, M. D.; Yang, Y. S.; Solomon, E. I.; Enemark, J. H. *Inorg. Chem.* **2001**, *40*, 687.
(11) McMaster, J.; Enemark, J. H. *Curr. Opin. Chem. Biol.* **1998**, *2*, 201.
(12) Gorman, C. B.; Smith, J. C. *J. Am. Chem. Soc.* **2000**, *122*, 9342.
(13) Gorman, C. B.; Smith, J. C.; Hager, M. W.; Parkhurst, B. L.; Sierzputowskagracz, H.; Haney, C. A. *J.* Am. Chem. Soc. **1999**, *121*, 9958.
(14) Basu, P.; Nemykin, V. N.; Sengar, R. S. *Inorg. Chem.* **2003**, *42*, 7489.
(15) Boyd, I. W.; Dance, I. G.; Murray, K. S.; Wedd, A. G. *Aust. J. Chem.* **1978**, *31*, 279.
(16) Frisch, M. J.; Trucks, G. W.; Schlegel, H. B.; Scuseria, G. E.; Robb, M. A.; Cheeseman, J. R.; Zakrzewski, V. G.; Montgomery, J. A., Jr.; Stratmann, R. E.; Burant, J. C.; Dapprich, S.; Millam, J. M.; Daniels, A. D.; Kudin, K. N.; Strain, M. C.; Farkas, O.; Tomasi, J.; Barone, V.; Cossi, M.; Cammi, R.; Mennucci, B.; Pomelli, C.; Adamo, C.; Clifford, S.; Ochterski, J.; Petersson, G. A.; Ayala, P. Y.; Cui, Q.; Morokuma, K.; Malick, D. K.; Rabuck, A. D.; Raghavachari, K.; Foresman, J. B.; Cioslowski, J.; Ortiz, J. V.; Baboul, A. G.; Stefanov, B. B.; Liu, G.; Liashenko, A.; Piskorz, P.; Komaromi, I.; Gomperts, R.; Martin, R. L.; Fox, D. J.; Keith, T.; Al-Laham, M. A.; Peng, C. Y.; Nanayakkara, A.; Gonzalez, C.; Challacombe, M.; Gill, P. M. W.; Johnson, B.; Chen, W.; Wong, M. W.; Andres, J. L.; Gonzalez, C.; Head-Gordon, M.; Replogle, E. S.; Pople, J. A. *Gaussian 98*, revision A.7; Gaussian, Inc.: Pittsburgh, PA, 1998.

basis set for all nonmetal atoms with a polarization function added for oxygen and sulfur atoms. The LANL2DZ basis set and LANL2 effective core potential were used for molybdenum. These computational conditions have repeatedly provided results consistent with experiment for mononuclear oxomolybdenum systems.[8,17−20] Geometry optimizations were performed on the computational model $[MoO(SCH_3)_4]^{-/2-}$ using SCH_3^- in place of the benzenethiolate ligands and initial geometric parameters for the $MoOS_4C_4$ core were obtained from averaged values of the $[Ph_4As][MoO(SPh)_4]$ crystal structure idealized to C_2 symmetry.[21] Frequency calculations were performed simultaneously to ensure the optimization converged to a minimum. An open-shell spin-unrestricted formalism was used for Mo^V calculations, while closed-shell spin-restricted calculations were performed for the Mo^{IV} complex. Calculations in CH_3CN solution were performed using the Onsager solvent model with solvent sphere radii calculated using the volume keyword as implemented in the Gaussian 98 program (4.96 Å for Mo^V and 5.06 Å for Mo^{IV}); otherwise, all calculations were in vacuo.

Results and Analysis

Electronic Absorption and Magnetic Circular Dichroism (MCD) Spectroscopy. The electronic absorption spectra of $[MoO(SPh)_4]^-$, **1**, **1CN**, and **1E** are overlayed in Figure 2. The spectra are generally similar, displaying a broad charge transfer feature with a maximum at approximately 16 000 cm^{-1} and a trough around 20 000 cm^{-1}, followed by intense absorption at higher energies. These spectral features are decidedly characteristic of monooxo Mo^V tetrathiolate complexes.[8,10,15,22−28] The broad low-energy spectral features of **1**, **1CN**, and **1E** span the 12 000−19 000 cm^{-1} energy region with the single maximum observed at 16 180 cm^{-1} for **1** ($\epsilon \approx 4800$ M^{-1} cm^{-1}), 16 500 cm^{-1} for **1CN** ($\epsilon \approx 5390$ M^{-1} cm^{-1}), and 16 400 cm^{-1} for **1E** ($\epsilon \approx 5840$ M^{-1} cm^{-1}). A very broad and increasingly intense absorption envelope is present above 20 000 cm^{-1} with a weakly defined shoulder at ~22 000 cm^{-1} ($\epsilon \approx 4000$ M^{-1} cm^{-1}) and a well-defined higher energy shoulder at ~28 500 cm^{-1} ($\epsilon \approx$ 20 000−30 000 M^{-1} cm^{-1}). The most pronounced difference in the **1**, **1CN**, and **1E** spectra relative to the $[MoO(SPh)_4]^-$ spectrum is observed in the high-energy region. The shoulder observed in the **1**, **1CN**, and **1E** spectra at ~28 500 cm^{-1} is more intense and ~1500 cm^{-1} lower in energy than the ~30 000 cm^{-1} ($\epsilon \approx 13$ 000 M^{-1} cm^{-1}) shoulder observed in the spectrum of $[MoO(SPh)_4]^-$. The apparent greater intensity observed above 20 000 cm^{-1} for the three *para*-substituted complexes compared to that of $[MoO(SPh)_4]^-$ is likely due to Rayleigh scattering effects, which possess a ν^4 dependence.

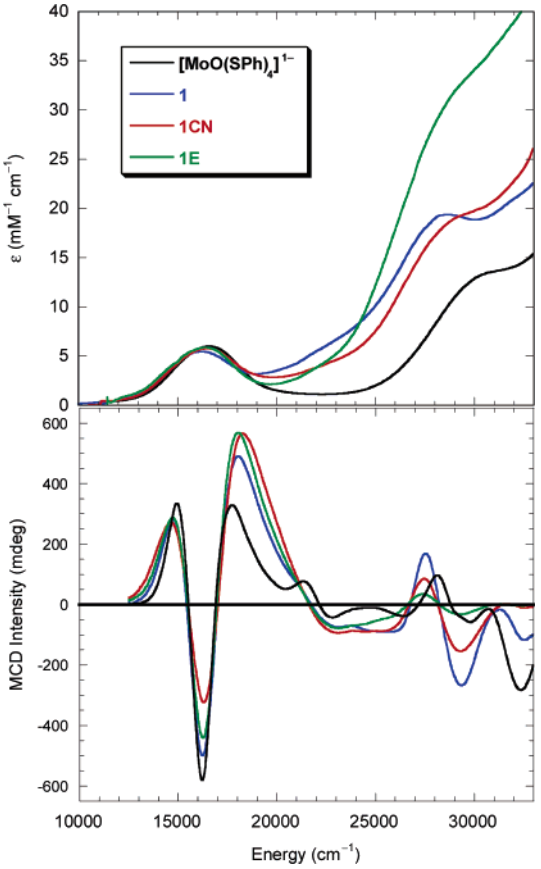

Figure 2. Electronic absorption (top) and MCD (bottom) spectra of **1**, **1CN**, **1E**, and $[MoO(SPh)_4]^-$.

The 5 K/7 T MCD spectra of $[MoO(SPh)_4]^-$, **1**, **1CN**, and **1E** are presented in Figure 2. The spectral band shapes and energies are similar for these complexes throughout the entire spectral region, but some broadening of the bands is observed for **1**, **1CN**, and **1E**. Three bands with a positive−negative−positive band pattern are present in the 12 000−19 000 cm^{-1} energy region, corresponding to the envelope of the broad low-energy absorption feature in both spectra. The energies of the bands are nearly identical for all four complexes below 27 000 cm^{-1}. The high-energy pseudo-A term band in the spectra of **1**, **1CN**, and **1E** is observed at 28 200 cm^{-1}, clearly shifted ~1000 cm^{-1} to lower energy than the pseudo-A term in the $[MoO(SPh)_4]^-$ spectrum, analogous to the differences observed in the absorption spectra.

The similarity of the electronic absorption and MCD spectra of **1**, **1CN**, and **1E** to that observed for $[MoO(SPh)_4]^-$ allow the spectral band assignments previously determined for $[MoO(SPh)_4]^-$ to also be applied to the spectra of **1**, **1CN**, and **1E**.[8,10] Furthermore, the electronic structure and resultant molecular orbital energies of **1**, **1CN**, and **1E** are also analogous to those determined for $[MoO(SPh)_4]^-$. The dominant oxomolybdenum−thiolate orbital interactions are depicted in Figure 3. The strong splitting of the oxomolybdenum ligand field results in the energetic isolation of the formal

(17) McNaughton, R. L.; Helton, M. E.; Cosper, M. M.; Enemark, J. H.; Kirk, M. L. *Inorg. Chem.* **2004**, *43*, 1625.
(18) McNaughton, R. L.; Helton, M. E.; Rubie, N. D.; Kirk, M. L. *Inorg. Chem.* **2000**, *39*, 4386.
(19) Peariso, K.; McNaughton, R. L.; Kirk, M. K. *J. Am. Chem. Soc.* **2002**, *124*, 9006.
(20) Rubie, N. D.; Peariso, K.; Doonan, C. J.; George, G. N.; Young, C. G.; Kirk, M. L. Submitted for publication.
(21) Bradbury, J. R.; Mackay, M. F.; Wedd, A. G. *Aust. J. Chem.* **1978**, *31*, 2423.
(22) Hanson, G. R.; Brunette, A. A.; Mcdonell, A. C.; Murray, K. S.; Wedd, A. G. *J. Am. Chem. Soc.* **1981**, *103*, 1953.
(23) Ueyama, N.; Yoshinaga, N.; Kajiwara, A.; Nakamura, A. *Chem. Lett.* **1990**, 1781.
(24) Ueyama, N.; Zaima, H.; Nakamura, A. *Chem. Lett.* **1986**, 1099.
(25) Ueyama, N.; Zaima, H.; Nakamura, A. *Chem. Lett.* **1985**, 1481.
(26) Ellis, S. R.; Collison, D.; Garner, C. D. *J. Chem. Soc., Dalton Trans.* **1989**, 413.
(27) Soong, S. L.; Chebolu, V.; Koch, S. A.; O'Sullivan, T.; Millar, M. *Inorg. Chem.* **1986**, *25*, 4067.
(28) Bradbury, J. R.; Masters, A. F.; Mcdonell, A. C.; Brunette, A. A.; Bond, A. M.; Wedd, A. G. *J. Am. Chem. Soc.* **1981**, *103*, 1959.

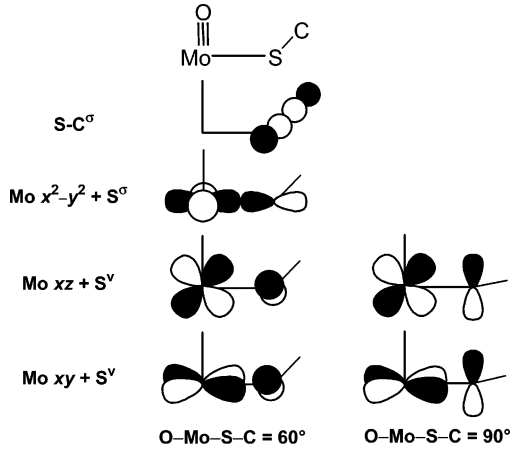

Figure 3. Primary orbital interactions in oxomolybdenum−benzenethiolate complexes. Note that one sulfur 3p orbital bonds to the carbon of the phenyl ring, another (S^{σ}) forms a σ bond with $d_{x^2-y^2}$, and the third (S^{v}) can interact with d_{xz}, d_{yz}, and the d_{xy} redox orbital depending on the O−Mo−S−C dihedral angle.

Mo d_{xy} orbital, which is the singly occupied redox orbital in the Mo^{V} oxidation state.[29−31] It is known that the intense low-energy absorption feature observed in $[MoO(SPh)_4]^-$ arises predominantly from three overlapping $S^{v} \rightarrow$ Mo d_{xy} LMCT transitions, while the higher energy absorption intensity is dominated by S → Mo $d_{xz,yz}$ LMCT transitions.[8] The intensities of the S → Mo LMCT features provide a probe of the covalency[32] between the molybdenum d_{xy}, d_{xz}, and d_{yz} orbitals and the thiolate ligand S^{v} orbital, which are *directly* dependent on the O−Mo−S−C dihedral angle (Figure 3).[8,10,17,33,34]

Electronic Structure Calculations. DFT calculations were performed on $[Mo^{V}O(SCH_3)_4]^-$ and $[Mo^{IV}O(SCH_3)_4]^{2-}$, computational models for the $[Mo^{V}OS_4]^-$ cores and the one-electron-reduced $[Mo^{IV}OS_4]^{2-}$ species, respectively. Geometry optimization calculations were performed both in vacuo and in CH_3CN solvent using C_2 symmetry, which allowed for possible low-symmetry distortions from the idealized C_4 core, as there is evidence for such low-symmetry distortions in the literature.[35] The resulting optimized bond lengths and angles are listed in Table 1, where S1 and S2 denote distinct sulfur atoms in the C_2 geometry. The Mo^{V} model optimized to nearly ideal C_4 symmetry, but the Mo^{IV} optimized geometry displays a distortion toward C_2 symmetry in both the O−Mo−S and O−Mo−S−C angles. Calculations on both the oxidized and reduced computational models slightly overestimate the bond lengths compared to the crystal structure values, a trend often observed for DFT-calculated geometries of transition metal complexes, but the average bond angles compare well with the crystal structure values. The most substantial difference between the Mo^{IV} and Mo^{V} geometries is observed in the O−Mo−S−C dihedral angles for both the experimental (∼25°) and DFT-calculated (∼32°) geometries.

The in vacuo and CH_3CN solvated optimization calculations show the expected splitting of the oxomolybdenum ligand field that results in the energetic isolation of the formal Mo d_{xy} orbital. This d_{xy} orbital is the redox orbital and is singly occupied in the Mo^{V} oxidation state and doubly occupied upon one-electron reduction of the site.[30,31] A comparison of the atomic orbital character contributing to the formal molybdenum d orbitals in the Mo^{V} and Mo^{IV} oxidation states is listed in Table 2. The total amount of sulfur character remains constant for the σ-bonding $d_{x^2-y^2}$ and d_{z^2} orbitals, whereas the sulfur character contributing to the π-bonding and pseudo σ-bonding d_{xz}, d_{yz}, and d_{xy} orbitals decreases by more than a factor of 2 in the Mo^{IV} optimized geometry relative to the Mo^{V} optimized geometry. The ability of the soft thiolate donor ligands to modulate the change in the effective nuclear charge on molybdenum that accompanies one-electron reduction is clearly observed in Figure 4, where the Mo d_{xy} contribution to the redox orbital increases substantially in the reduced Mo^{IV} state. This anisotropic differential covalency trend is also observed for the oxygen atomic orbital character contributing to the molecular orbitals. Again, the total oxo contribution to the σ-bonding orbitals ($d_{x^2-y^2}$, d_{z^2}) remains constant while the total oxo contribution to the d_{xy}, d_{xz}, and d_{yz} orbitals decreases by a factor of 2 in the reduced geometry. This change in sulfur and oxygen atomic orbital character contributing to the molecular orbitals as a function of molybdenum oxidation state is clearly apparent in the contour plots shown in Figure 4. However, inspection of the Mulliken charges on sulfur and oxygen (Table 3) implies that the thiolate sulfur donor ligands are much more affected by reduction than the oxo ligand, as shown by the nearly 2-fold increase in negative charge per sulfur compared to the oxo ligand. This reflects the hard donor nature of the terminal oxo ligand and the inability of this ligand to effectively buffer the $[MoO(SR)_4]^{-/2-}$ site against the electronic and geometric structure changes that accompany reduction. In summary, changes in metal−ligand covalency contributions to the formal d_{xy}, d_{xz}, and d_{yz} molecular orbitals are dominated by changes in Mo−S bonding, with a substantial decrease in Mo−S covalency upon reduction of the $[MoO(SCH_3)_4]^-$ model.

The effect of solvation on the geometry, total energy, molecular orbital energies, Mulliken charges, and dipole moments of $[MoO(SCH_3)_4]^-$ and $[MoO(SCH_3)_4]^{2-}$ was explored using acetonitrile as solvent. No change in the bond lengths were observed to result from solvation effects, and changes in the bond angles averaged less than 0.4° (Table 1). The total-energy stabilization incurred by the computational models due to solvation was found to be small, amounting to −0.014 and −0.007 eV (1.30 and 0.67 kJ/mol) for the optimized Mo^{V} and Mo^{IV} geometries, respectively (Table 3). Additionally, the Mulliken charges of the molybdenum as well as those of the donor atoms are not greatly affected upon solvation. An attempt was made to evaluate the contribution of solvent to the electronic stabi-

(29) Nugent, W. A.; Mayer, J. M. *Metal-Ligand Multiple Bonds*; Wiley & Sons: New York, 1988.
(30) Sabel, D. M.; Gewirth, A. A. *Inorg. Chem.* **1994**, *33*, 148.
(31) Lever, A. B. P. *Inorganic Electronic Spectroscopy*; Elsevier Science Publishing: New York, 1986.
(32) Solomon, E. I. *Comments Inorg. Chem.* **1984**, *5*, 225.
(33) McNaughton, R. L.; Helton, M. E.; Cosper, M. M.; Enemark, J. H.; Kirk, M. L. *Inorg. Chem.* **2004**, *43*, 1625.
(34) Helton, M. E.; Kirk, M. L. Manuscript in preparation.
(35) Kondo, M.; Ueyama, N.; Fukuyama, K.; Nakamura, A. *Bull. Chem. Soc. Jpn.* **1993**, *66*, 1391.

Table 1. Comparison of DFT Calculated and Crystallographically Determined Bond Lengths and Angles for $[MoO(SR)_4]^{-/2-}$

	$[Mo^VO(SR)_4]^-$			$[Mo^{IV}O(SR)_4]^{2-}$			$\Delta(Mo^{IV}-Mo^V)$		
param	exptl[a]	$calcd_{gs}$[b]	$calcd_{sol}$[c]	exptl[d]	$calcd_{gs}$[b]	$calcd_{sol}$[c]	exptl	$calcd_{gs}$	$calcd_{sol}$
				Bond Lengths (Å)					
Mo−O	1.67	1.70	1.70	1.69	1.71	1.71	0.02	0.01	0.01
Mo−S1	2.40	2.46	2.46	2.41	2.51	2.51	0.01	0.05	0.05
Mo−S2	2.41	2.46	2.46	2.43	2.50	2.50	0.02	0.04	0.04
				Bond Angles (deg)					
Mo−S1−C	109.5	107.5	107.3	115.5	112.6	112.7	6.0	5.1	5.4
Mo−S2−C	110.1	108.0	107.6	117.0	113.8	114.0	6.9	5.8	6.4
O−Mo−S1	110.8	108.9	108.7	109.7	104.3	104.4	−1.1	−4.6	−4.3
O−Mo−S2	109.0	109.4	109.4	105.8	107.3	107.2	−3.2	−2.1	−2.2
O−Mo−S1−C	58.7	54.7	54.3	80.8	83.7	84.3	22.1	29.0	30.0
O−Mo−S2−C	58.3	55.7	54.4	86.1	89.0	90.0	27.8	33.3	35.6

[a] Reference 21. [b] In vacuo calculation. [c] CH_3CN-solvated calculation. [d] Reference 35.

Table 2. Atomic Orbital Character (%) Contributing to the Formal Mo d Orbitals of $[MoO(SCH_3)_4]^{-/2-}$

	$[Mo^VO(SCH_3)_4]^-$				$[Mo^{IV}O(SCH_3)_4]^{2-}$			
orbital	Mo	O	S1	S2	Mo	O	S1	S2
d_{xy}	46.7	0.0	19.6	20.1	68.3	0.0	8.1	9.2
d_{yz}	49.1	13.4	31.4	0.5	69.9	5.4	0.5	10.2
d_{xz}	48.9	13.3	0.5	31.6	66.3	6.4	13.7	0.6
$d_{x^2-y^2}$	37.2	0.1	9.2	28.7	41.7[a]	4.2	31.8	13.5
d_{z^2}	55.4	14.9	7.6	11.5	46.3[a]	9.5	7.4	28.8

[a] These orbitals mix as $d_{x^2-y^2} + d_{z^2}$.

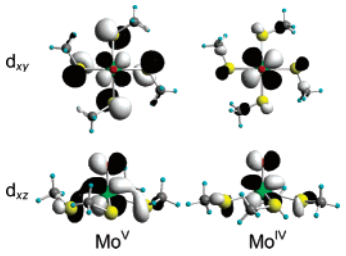

Figure 4. Molecular orbital contours of the d_{xy} and d_{xz} orbitals resulting from geometry optimization DFT calculations on $[Mo^VO(SCH_3)_4]^-$ and $[Mo^{IV}O(SCH_3)_4]^{2-}$. The d_{yz} orbitals are rotated 90° relative to the d_{xz} orbitals but otherwise appear identical. Note the decrease in sulfur atomic orbital character in both of the Mo^{IV} orbitals and the expansion of the molybdenum atomic orbital in the doubly occupied Mo^{IV} d_{xy} orbital relative to the singly occupied Mo^V d_{xy} orbital.

lization of the reduced Mo^{IV} site, in the absence of geometric reorganizational effects, by computing the single-point energy of the Mo^{IV} computational model with the Mo^V optimized geometry in both the in vacuo and CH_3CN-solvated states. The solvent-induced stabilization of the reduced Mo^{IV} state at the Mo^V geometry is calculated to be only −0.008 eV. Furthermore, the molybdenum Mulliken charges and energies of the redox orbitals are identical for the in vacuo phase and in CH_3CN at the Mo^V geometry. When the total energies of the Mo^{IV} single point calculations are compared to the corresponding Mo^{IV} calculations performed at the optimized Mo^V geometry, a remarkably large 0.44 eV total energy stabilization is observed. This energy stabilization is significant, as it is ∼55 times that of the calculated solvent stabilization of the Mo^{IV} without the effect of geometric relaxation. Thus, the dominant contribution to stabilization of the reduced Mo^{IV} model appears to be a structural reorganization along a low-frequency torsional vibrational coordinate, and this manifests itself in an ∼30° increase (opening) of the O−Mo−S−C dihedral angle.

Figure 5 depicts the Mulliken charge on the sulfur atoms of *p*-$SPhCONHCH_3^-$ and SPh^- and plots of the two highest energy occupied molecular orbitals, which are the donor orbitals, for each ligand. The calculated Mulliken charges on the sulfur atom reflect the relative electron-donating abilities of the ligands used in this study.[47] The presence of an electron-withdrawing amide substituent results in a 0.073 decrease of the negative charge on the sulfur donor atom, indicating that *p*-$SPhCONHCH_3^-$ is a poorer electron donor than SPh^-. The nature of the S^v orbital in *p*-$SPhCONHCH_3^-$ and SPh^- is essentially identical, reflecting the fact that there is no appreciable electron density contribution to this ligand orbital from the *para* substituent.[36] This is an important observation because the S^v orbital is the thiolate ligand orbital that primarily interacts with the formal molybdenum d_{xy} orbital. In contrast, the electron-withdrawing *para* substituent contributes substantially to the electron density present in the S^σ ligand molecular orbital, which is primarily involved in σ-bonding with the formal Mo $d_{x^2-y^2}$ orbital and, to a lesser degree, the Mo d_{z^2} orbital.[36] Therefore, these results suggest that differences in the electronic structures of $[MoO(SPh)_4]^-$ and $[MoO(p\text{-}SPhCONHR)_4]^-$ complexes are not dominated by differential d_{xy} HOMO stabilization, which is supported by the similar energies of the $S^v \rightarrow d_{xy}$ LMCT transition energies for these complexes in the electronic absorption and MCD spectra. The primary differences in $[MoO(SPh)_4]^-$ and $[MoO(p\text{-}SPh\text{-}CONHR)_4]^-$ electronic structures appear to result from substituent-mediated changes in the composition and energy of the $d_{x^2-y^2}$ and d_{z^2} virtual orbitals. These orbitals should be more destabilized for $[MoO(SPh)_4]^-$ due to the greater charge donation of the S^σ orbital in SPh^- with $d_{x^2-y^2}$ and d_{z^2}. The reduced donating ability of the sulfur atom in *p*-$SPhCONHCH_3^-$ will result in a more positive effective nuclear charge on the molybdenum ion in the $[MoO(p\text{-}SPhCONHR)_4]^-$ complexes, which should lead to more positive reduction potentials for the $[MoO(p\text{-}SPhCONHR)_4]^-$ complexes when compared to $[MoO(SPh)_4]^-$.

Discussion

In general, the electronic absorption and MCD spectra of **1**, **1CN**, and **1E** are very similar to those typically observed for oxomolybdenum tetrathiolate complexes. In fact, numer-

(36) The S^v and S^σ orbital notation is shown in Figure 3 and explained thoroughly in ref 8.

Table 3. Comparison of Output Parameters of DFT Computations on $[MoO(SCH_3)_4]^{-/2-}$

Mo oxidn state	computatnl method	tot. energy (eV)	Mulliken charges			energy of d_{xy} redox orbital (eV)	dipole moment along *z*-axis (D)[b]
			Mo	O	S[a]		
5	in vacuo geometry optimizatn	−51 574.41 2	0.300	−0.504	−0.581	−1.394	2.454
5	CH_3CN-solvated geometry optimizatn	−51 574.42 6	0.305	−0.497	−0.607	−1.403	2.910
4	in vacuo geometry optimizatn	−51 572.41 0	0.288	−0.543	−1.160	3.113	−0.413
4	CH_3CN-solvated geometry optimizatn	−51 572.41 7	0.285	−0.547	−1.154	3.103	−0.708
4	in vacuo single point at Mo^V geometry	−51 571.96 9	0.267	−0.571	−1.148	3.945	2.709
4	CH_3CN-solvated single point at Mo^V geometry	−51 571.97 7	0.267	−0.564	−1.171	3.945	3.166

[a] Sum of all 4 sulfur charges in the molecule. [b] The *z*-axis is oriented along the Mo≡O bond. The *x* and *y* components of the dipole moment are zero so this value is also the molecular dipole moment.

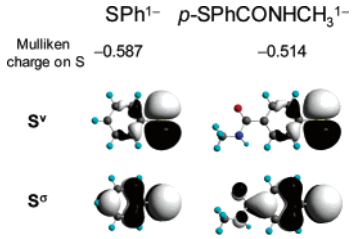

Figure 5. DFT-calculated Mulliken charges and molecular orbital contours of the two highest energy occupied molecular orbitals of SPh^- and *p*-$SPhCONHCH_3^-$ ligands.

ous other *para*-substituted oxomolybdenum tetrathiolate complexes exhibit electronic absorption, MCD, and even EPR spectra that are nearly identical with the spectra of $[MoO(SPh)_4]^-$.[8,10,15,21−27] Thus, the basic electronic structure and spectral band assignments previously determined for these complexes can also be applied to **1**, **1CN**, and **1E**. It is known that the intensity of the low-energy S → Mo LMCT feature provides a probe of the covalency between the molybdenum d_{xy} orbital and the thiolate ligand S^v orbitals[32] and is *directly* dependent on the O−Mo−S−C dihedral angle.[8,10,17,33,34] A strong π-type orbital interaction occurs when the O−Mo−S−C dihedral angle is near 0° (or 180°), and this covalent bonding interaction is reduced until the interaction is nonbonding when the dihedral angle approaches 90°. The key concept here is that the degree of thiolate sulfur electron density covalently delocalized onto the molybdenum ion is primarily regulated by the geometry of the thiolate ligands. Since the energies and intensities of the low-energy S → Mo LMCT excitations are very similar for all four of the complexes presented in this study, it follows that their O−Mo−S−C dihedral angles are also similar.

The only noteworthy difference apparent in the electronic absorption and MCD spectra of **1**, **1CN**, and **1E** compared to $[MoO(SPh)_4]^-$ is the ∼1000 cm^{-1} shift of the higher energy S^σ → Mo $d_{xz,yz}$ charge-transfer transitions observed for each of the three *para*-substituted complexes. This spectral shift indicates that the S^σ thiolate orbitals in the *para*-substituted complexes interact with the molybdenum d_{xz} and d_{yz} orbitals in such a way that they are slightly less electron donating with respect to the thiolate S^σ orbitals in $[MoO(SPh)_4]^-$. Substituent effects on the reduction potentials of related oxomolybdenum−dithiolene complexes have been shown to correlate with the calculated Mulliken charge on the sulfur atoms of the free anionic ligand.[37] Our DFT calculations on the thiolate ligand anions show a more positive Mulliken charge on the sulfur donor for *p*-$SPhCONHCH_3^-$ relative to SPh^-. Although charge-transfer spectroscopy demonstrates that the nature of the redox orbital of the $[MoO(p\text{-}SPhCONHR)_4]^-$ complexes and $[MoO(SPh)_4]^-$ are very similar, the effective nuclear charge on the molybdenum should be slightly more positive for the $[MoO(p\text{-}SPhCONHR)_4]^-$ complexes due to weaker $S^\sigma \rightarrow d_{x^2-y^2}$ and $S^\sigma \rightarrow d_{z^2}$ charge donation. As such, the *para* substitution in these systems should result in their being easier to reduce relative to $[MoO(SPh)_4]^-$. This is in fact observed, as the reduction potential of $[MoO(SPh)_4]^-$ is −1383 mV, which is ∼170, 132, and 136 mV more negative than the reduction potentials of **1**, **1CN**, and **1E**, respectively.[14] Note that since the shift of the high energy band is the same for all three of the $[MoO(p\text{-}SPhCONHR)_4]^-$ complexes, the *para* substitution cannot explain the observed differences in the reduction potentials of **1**, **1CN**, and **1E** *relative to one another*, in DMF.

Given the aforementioned spectroscopic evidence for identical electronic structure descriptions of **1**, **1CN**, and **1E**, the differences observed in their reduction potentials are worthy of comment. To evaluate the observed trend, we must consider the two primary factors that govern the reduction potential of transition metal complexes (eqs 1 and 2).[38,39]

$$E_{1/2} = \mathrm{IE} + \Delta U \quad (1)$$

$$\Delta U = U_{\mathrm{reduced}} - U_{\mathrm{oxidized}} \quad (2)$$

The first contribution to reduction potential is the intrinsic ionization energy (IE) of the complex, which is determined by the valence ionization energy of the redox orbital, the effective nuclear charge of the redox-active center, and any necessary electronic relaxation or redistribution (eq 1). The second factor is a correction term to the IE that is defined as a change in the potential (ΔU) resulting from outer-sphere reorganization of the environment surrounding the redox-active center, such as the solvent or a protein matrix, caused by the redox-induced change in the electric dipole of the redox-active center (eq 2). This change in potential is dependent on the dielectric constant of the medium surrounding the redox center as well as changes in the overall charge and size (radius) of the complex upon reduction. Solvent accessibility and reorientation have been suggested as possible mechanisms for the reduction potential shifts of

(37) Helton, M. E.; Gruhn, N. E.; McNaughton, R. L.; Kirk, M. L. *Inorg. Chem.* **2000**, *39*, 2273.
(38) Holm, R. H.; Kennepohl, P.; Solomon, E. I. *Chem. Rev.* **1996**, *96*, 2239.
(39) Bair, R. A.; Goddard, W. A. *J. Am. Chem. Soc.* **1978**, *100*, 5669.

dendrimer-encapsulated redox-active metal centers.[1] In this study, the dipole moment of these sterically encumbered oxomolybdenum tetrathiolate complexes is anticipated to be collinear with the strong, polar Mo≡O bond, and the magnitude of this dipole should be greater for a $[Mo^{V}O]^{3+}$ unit than for $[Mo^{IV}O]^{2+}$. This prediction is supported by the results of DFT calculations, where the magnitude of the dipole moment for the Mo^{V} computational model is ~5 times greater than that for the Mo^{IV} computational model (Table 3). As such, solvent-dipole−complex-dipole interactions are expected to stabilize the Mo^{V} state relative to the reduced Mo^{IV} state, providing a negative contribution to the reduction potential. Provided these sterically encumbered ligands allow equal access of solvent at the oxomolybdenum site, the ΔU term should be constant across the series and is not expected to play a dominant role in determining reduction potential differences between **1**, **1CN**, and **1E** in this solvent system. Therefore, we will focus on electronic structure contributions to the reduction potentials of **1**, **1CN**, and **1E**. One contribution to the IE term, the effective nuclear charge at the metal center, is not likely to contribute to reduction potential differences between **1**, **1CN**, and **1E** since all three complexes possess *para*-substituted benzenethiolate ligands with nearly identical donor properties. A second contribution to changes in the IE term, the energy of the redox orbital, can also be eliminated as the primary source of reduction potential differences. This is due to the fact that **1**, **1CN**, and **1E** possess nearly indistinguishable transition energies and intensities of the low-energy S → Mo LMCT bands, which probe the nature of the d_{xy} redox orbital directly. The remaining contribution to the IE term involves electronic relaxation of the redox-active molybdenum center upon reduction. This inner-sphere electronic relaxation can be coupled to significant changes in electronic structure as a result of redistribution of the electron density, a change in the coordination geometry, or both of these simultaneously.

A change in S → Mo charge donation is anticipated to be coupled to the reduction process to stabilize the reduced Mo^{IV} state, since Mo^{IV} is a poorer Lewis acid than Mo^{V}. This electron density redistribution is most efficient via distortions along the O−Mo−S−C dihedral angles, which effectively modulate the thiolate-mediated charge donation into the redox orbital. We suggest that a geometric reorientation involving changes in the O−Mo−S−C dihedral angles will become increasingly difficult with increasingly bulky thiolate donor ligands. Crystal structures of oxomolybdenum tetrathiolate complexes support this hypothesis since the only significant difference between the Mo^{V} and Mo^{IV} geometries is the ~25° change in the O−Mo−S−C dihedral angles.[21,35] DFT geometry optimization calculations also support this idea, resulting in an ~30° increase in the O−Mo−S−C dihedral angle upon reduction as compared to the Mo^{V} complexes. This torsional reorganization results in a more nonbonding interaction between the S^{v} orbitals and the Mo^{IV} d_{xy} orbital, decreasing thiolate ligand charge donation to the reduced Mo^{IV} and increasing stabilization of the redox orbital relative to the undistorted geometry. This is nicely illustrated in the electron density contours of Figure 4, which clearly show the difference in the thiolate sulfur character donated to the d_{xy} orbital as a function of oxidation state. In summary, marked reorganization of the $MoOS_4C_4$ core is anticipated to accompany reduction of monooxo Mo^{V} tetrathiolate complexes in a manner that decreases thiolate → molybdenum charge donation and increases stabilization of the reduced state.

Further evidence for the importance of a significant reorganization energy component in the reduction of $[Mo^{V}OSR_4]^{-}$ centers is provided by a comparison of $[MoO(SPh)_4]^{-}$ and $[MoO(SPh-PhS)_2]^{-}$.[8,40] These two oxomolybdenum thiolates possess very similar ligand-donating ability and nearly identical steric bulk, which should yield similar solvent accessibility at the molybdenum center. The constrained geometry of $[MoO(SPh-PhS)_2]^{-}$ is enforced by the biphenyl linkage in the $SPh-PhS^{2-}$ ligand, hindering thiolate ligand reorganization upon reduction of the Mo^{V} center and resulting in $[MoO(SPh-PhS)_2]^{-}$ being harder to reduce by ~120 mV relative to the unconstrained $[MoO(SPh)_4]^{-}$ complex. This result strongly supports the assertion that geometric reorganization is a key contributor to the reduction potentials of $[MoOSR_4]^{n-}$ centers. These studies suggest that an electronic buffer effect, analogous to that proposed for oxomolybdenum−dithiolene Mo−S bonding interactions in model complexes and pyranopterin molybdenum enzymes,[41,42] is also operative in oxomolybdenum−thiolates, albeit via a different mechanism. Redox processes which occur in oxomolybdenum−dithiolenes are effectively buffered against large changes in the effective nuclear charge of the molybdenum ion by a "folding" of the dithiolene ligand.[42−46] In contrast, changes in the effective nuclear charge of oxomolybdenum−thiolates appear to be effectively buffered by changes in the O−Mo−S−C dihedral angle. The demonstrated flexibility of the O−Mo−S−C linkage indicates that the cysteine thiolate ligand geometry in sulfite oxidase is likely to play a significant role in modulating oxomolybdenum−thiolate covalency and facilitating redox processes at the molybdenum center of this enzyme.

Acknowledgment. Support of this research by the National Institutes of Health (Grant Nos. GM-057378 to M.L.K. and GM-61555 to P.B.), Research Corp. (Grant RI 249 to P.B.), and The University of New Mexico Dean's Dissertation Fellowship to R.L.M. is gratefully acknowledged.

IC0482281

(40) Conry, R. R.; Tipton, A. A. *J. Biol. Inorg. Chem.* **2001**, *6*, 359.
(41) Westcott, B. L.; Gruhn, N. E.; Enemark, J. H. *J. Am. Chem. Soc.* **1998**, *120*, 3382.
(42) Kirk, M. L.; McNaughton, R. L.; Helton, M. E. *Prog. Inorg. Chem.* **2003**, *52*, 111.
(43) Joshi, H. K.; Inscore, F. E.; Schirlin, J. T.; Dhawan, I. K.; Carducci, M. D.; Bill, T. G.; Enemark, J. H. *Inorg. Chim. Acta* **2002**, *337*, 275.
(44) Joshi, H. K.; Cooney, J. J. A.; Inscore, F. E.; Gruhn, N. E.; Lichtenberger, D. L.; Enemark, J. H. *Proc. Natl. Acad. Sci. U.S.A.* **2003**, *100*, 3719.
(45) Joshi, H. K.; Enemark, J. H. *J. Am. Chem. Soc.* **2004**, *126*, 11784.
(46) Waters, T.; Wang, X.-B.; Yang, X.; Zhang, L.; O'Hair, R. A. J.; Wang, L.-S.; Wedd, A. G. *J. Am. Chem. Soc.* **2004**, *126*, 5119.
(47) Sengar, R. S.; Nemykin, V. N.; Basu, P. *New. Jour. Chem.* **2003**, *27*, 1115.